Progress In Electromagnetics Research C, Vol. 48, 77–86, 2014

A Modified Synchronization Method for Bistatic SAR

Yun Feng Shao*, Yue Liu, Run Chen, and Gang Liu

Abstract—It is a common synchronization approach of the bistatic Synthetic Aperture Radar (BiSAR) with spaceborne/stationary configuration that obtains synchronization information from a direct signal. An easy and effective synchronization method is using the direct signal as a match filter to compress the echo for range compression. This method requires a high signal-to-noise ratio (SNR) of the direct signal, because the low SNR of the direct signal affects the synchronization result. Furthermore, it affects the imaging quality and bistatic-InSAR (BiInSAR) result seriously. Two factors affect the SNR of the direct signal: low gain and saturation. The transmitter and receiver antenna beam patterns cause the received direct signal's power variance during the exposure time. The requirement of high gain and no saturation cannot be satisfied simultaneously during the exposure time when the receiver sub-system does not have automatic gain control (AGC). In this paper, a modified synchronization approach is proposed. The proposed method not only tolerates the low gain and saturation, but also does not require the parameters of the transmitted signal, such as FM chirp rate, bandwidth and transmitted pulse length. The proposed method makes the gain design of the synchronization channel easy. The experiment results verifies the effectiveness of the proposed approach.

1. INTRODUCTION

With its all-weather and all-time capabilities, the Synthetic Aperture Radar (SAR) has great potentials, such as in geology, forestry, agriculture and oceanography [1–6]. As a special mode, the bistatic SAR (BiSAR) systems have been attracting scientists' interests in the last few years, and a lot of BiSAR experiments have been carried out. BiSAR system has many advantages, including high flexibility in designing SAR missions, higher signal to noise ratio (SNR), etc. [7–20]. As a typical BiSAR configuration, spaceborne/stationary configuration fixes the transmitter sub-system on the satellite and the receiver sub-system on the ground, as shown in Figure 1. The ground receiver sub-system contains two types of channels. One is the synchronization channel, which directly receives chirp signal from the transmitter on the satellite, as channel A in Figure 1. Besides triggering the echo channels, the synchronization channel is also used to obtain synchronization information. The other is echo channel, which receives the echo from the ground, as channel B_n in Figure 1.

The spatial separation of transmitter and receiver makes synchronization the greatest challenge of BiSAR operation. The synchronization error is analyzed by many researchers, and some synchronization algorithms have recently been proposed. In [11], the frequency error between transmit carrier frequency and receiver oscillator's frequency is analyzed. The chirp ratio error and nonlinear phase error were considered in [12]. Those errors affect integrated side-lobe ratio (ISLR), reduce azimuth resolution and shift targets along the range direction [13]. Literature [14] established error transfer model from the error of the time and frequency synchronization to the error of interferometric phase. Literature [15] proposed a method using oscillator strained by Global Position System (GPS), ultra-high-quality oscillators, a direct exchange of radar pulses and an appropriate bidirectional link. But none of these strategies

Received 20 November 2013, Accepted 8 March 2014, Scheduled 12 March 2014

* Corresponding author: Yun Feng Shao (shao-yun-feng@163.com).

The authors are with the Department of Space Microwave Remote Sensing System, Institute of Electronics, Chinese Academy of Sciences, Beijing 100190, China.

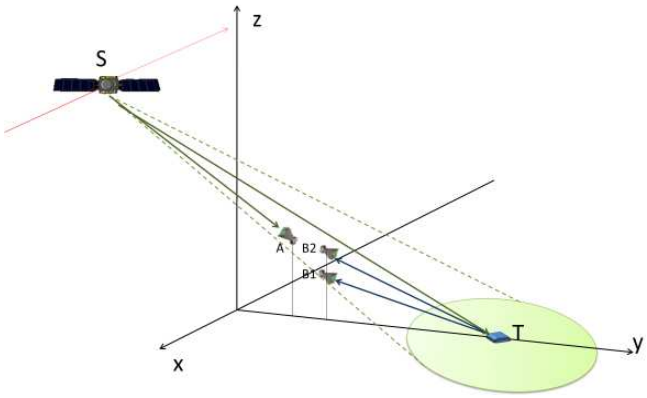

Figure 1. The geometry of the Bi-static SAR configuration [10].

can be applied directly if the receiver uses a non-cooperative source of opportunity [16, 17]. Reference target is used in [18] to achieve synchronization. A dedicated channel that receives signal directly from transmitter can also provide synchronization information [16–19]. However, the above-mentioned methods have limitation in practice when the parameters of the transmitted signal are unknown, and the direct signal has serious saturation, or the gain of the direct signal (GDS) is very low. The parameters of the transmitted signal include FM chirp rate, bandwidth and transmitted pulse length. Though the parameters of the transmitted signal can be estimated from the direct signal, the estimation results are not precise enough to be used in BiInSAR processing when the saturation is very serious, or the GDS is very low. Another useful method to solve the synchronization problem is to compress the received echo by using the signal received by the synchronization receiver as a match filter. This method does not need to estimate the parameters of the chirp signal. Based on the synchronization method, a fast back-projection algorithm was proposed in [20]. However, this method required high SNR of the direct signal, which is hard to obtain for two reasons. Firstly, the pattern of the transmitter antenna and the receiver antenna caused variation of the direct signal power during the exposure time, when the receiver did not have Automatic Gain Control (AGC).

Figure 2 shows magnitude's variation of the received direct signal during the exposure time. The change is significant in the mainlobe. It is hard to compromise no saturation at the center of the mainlobe and high gain at the edge of the mainlobe. Both saturation at the center of the mainlobe and low gain at the edge of the mainlobe reduce the SNR. In this paper, we define a direct signal with saturation and/or low gain as unsatisfactory direct signal. Secondly, because of attenuation of the atmosphere, the power of the direct signal cannot be computed accurately. So the lower gain at edge of the mainlobe and saturation at the center of the mainlobe cannot be avoided in practice.

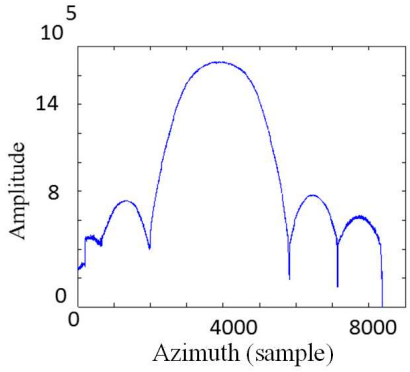

Figure 2. The amplitude of the received direct signal.

Figure 3 to Figure 5 show the different amplitudes of the sample value at intermediate frequency (IF) sampling (Figures (a)), the spectrum of the IF sampling (Figures (b)) and the spectrum of the demodulation complex signal (Figures (c)). The value of analog to digital converter (ADC) has 8 bit, so the maximum value of ADC is 128, and the minimum value of ADC is −127. Figure 3 shows the case of appropriate gain of the receiver. The SNR can reach 27 dB, which is high enough for a matched filter. Figure 4 shows the case with high GDS, where saturation exists, and the SNR reduces to 6 dB. Figure 5 shows the case with extremely high GDS and serious saturation. Figure 6 shows the case with low GDS. Though there is no saturation, SNR is lower than the appropriate GDS. The low GDS reduces 6 dB of SNR, which affects the SNR of the imaging result and BiInSAR results. All these experiment results verify the conclusion that the SNR of the unsatisfactory direct signal is low.

In this paper, a modified approach is proposed to solve the synchronization problem when the parameters of the chirp are unknown, and there exists an unsatisfactory direct signal. In Section 2, the synchronization method is proposed. Experiments are presented to verify the proposed method in Section 3.

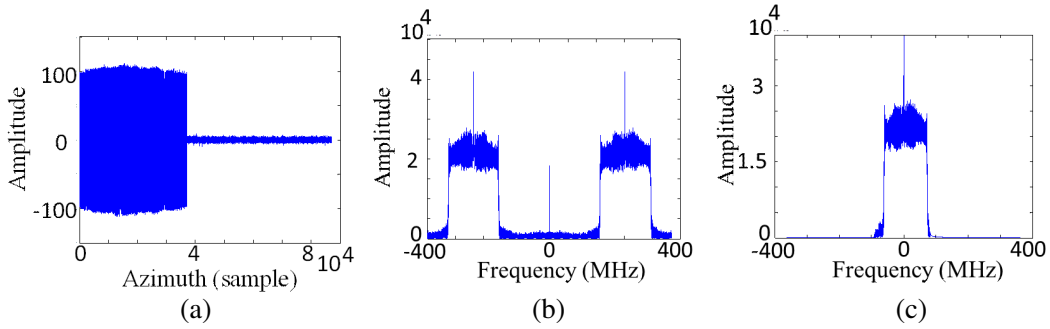

Figure 3. Appropriate gain. (a) Sample value at IF sampling. (b) Spectrum of the IF sampling. (c) Spectrum of the demodulation complex signal.

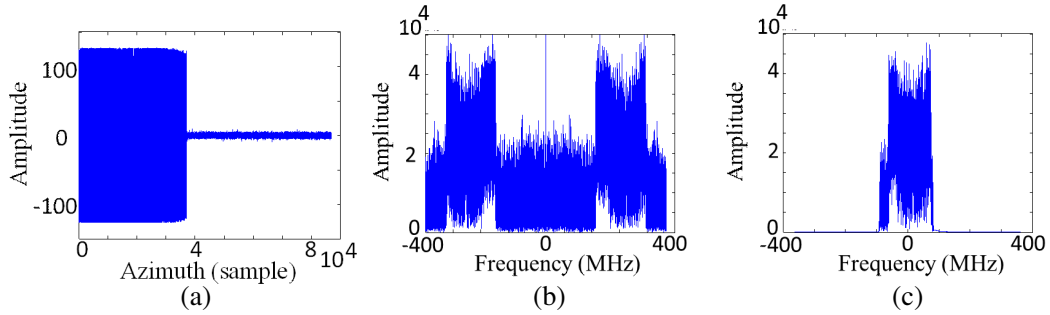

Figure 4. High gain with low saturation. (a) Sample value at IF sampling. (b) Spectrum of the IF sampling. (c) Spectrum of the demodulation complex signal.

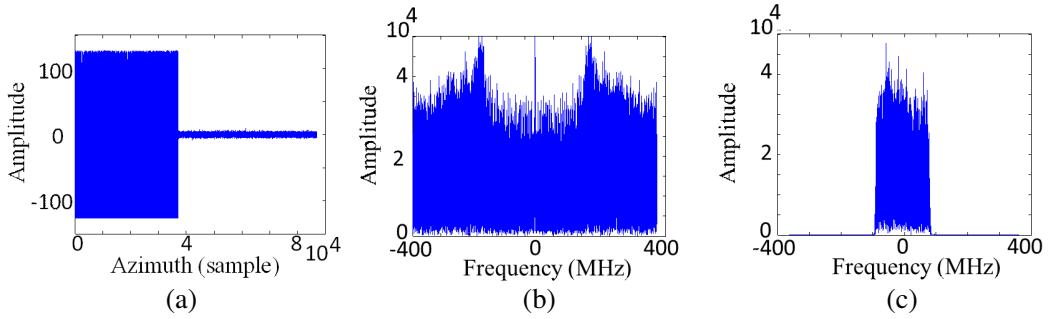

Figure 5. Extreme high gain with serious saturation. (a) Sample value at IF sampling. (b) Spectrum of the IF sampling. (c) Spectrum of the demodulation complex signal.

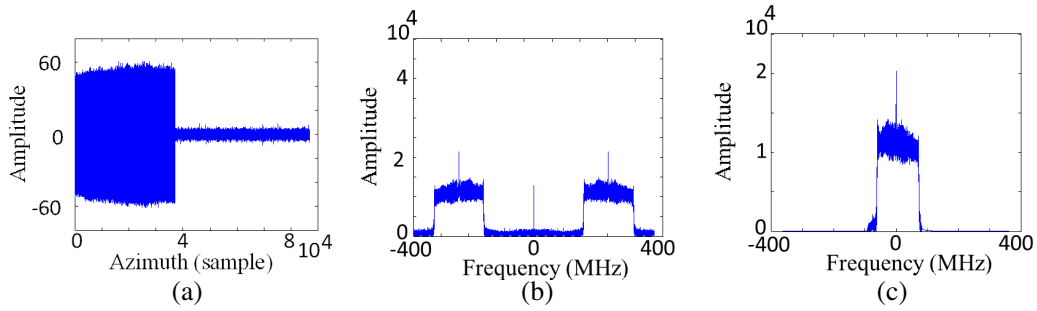

Figure 6. Low gain. (a) Sample value at IF sampling. (b) Spectrum of the IF sampling. (c) Spectrum of the demodulation complex signal.

2. ALGORITHM

2.1. Introduction of the Ground Receiver Sub-System

Figure 7(a) shows the block diagram of the ground receivers. The working mode of the system is as follows, as shown in Figure 7(b). The receiver system has two states: monitor state and record state. At the monitor state, the synchronization channel and echo channel only sample the received signal without recording data. At the record state, the synchronization channel and echo channel sample and record the received signal. From the beginning, the state of the receiver is a monitor state. When the synchronization channel detects the chirp signal, the state of the receiver translates into record state. The receiver holds the record state for a fixed time, which is shorter than pulse repetition interval, then it translates into the monitor state.

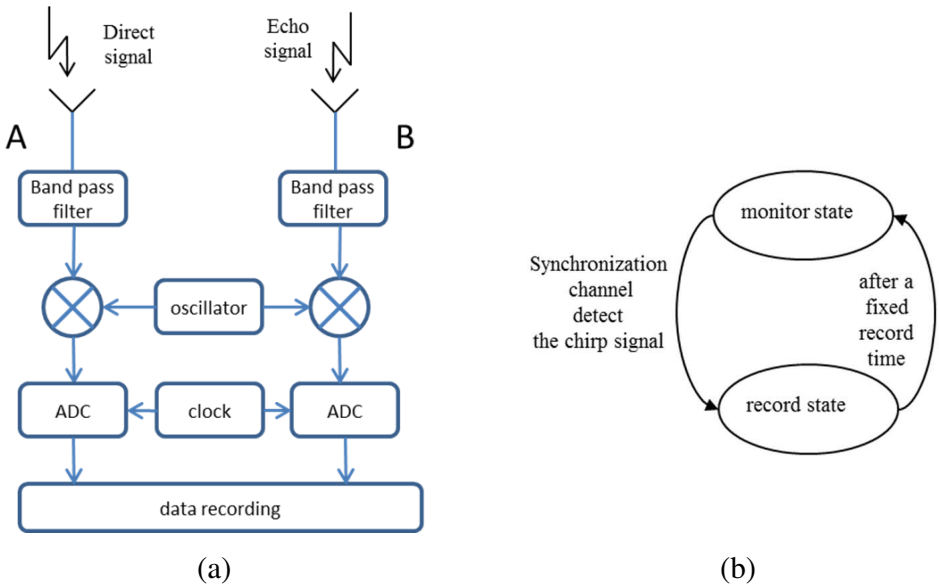

Figure 7. Receiver system. (a) Block diagram of the ground receivers. (b) Block diagram of states translation.

Due to the noise and attenuation as the chirp signal passes through aerosphere, the amplitude of chirp signal changes when it arrives at the synchronization channel, which means that the first several chirp pules cannot trigger the receiver system to the record state. Because the synchronization channel and echo channels use the same trigger signal, they share the same trigger delay time.

2.2. Theoretic Analysis

Figure 8 shows the block diagram of the proposed synchronization approach. Compared with the algorithm proposed in [20], two steps are added: choosing the reference direct signal and constructing the match filter, shown as red parts in Figure 8. Those steps are used to deal with unsatisfactory direct signal. The bold arrows represent data of all range lines and the unbold arrows represent data of only one range line.

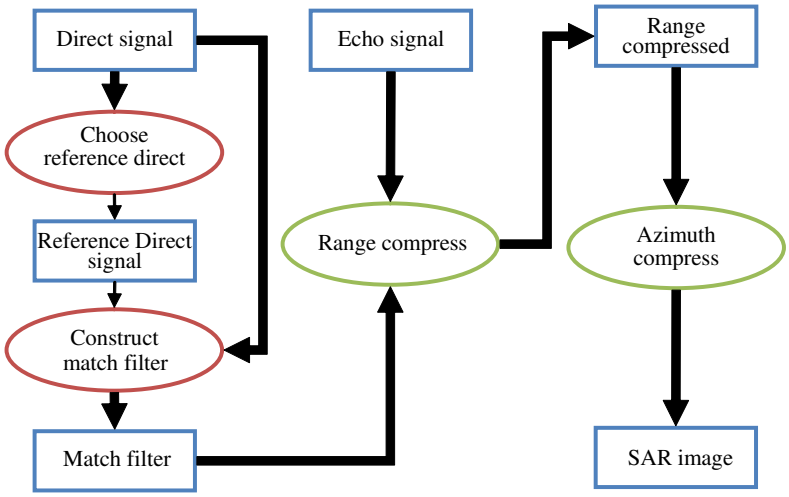

Figure 8. Block diagram of the proposed synchronization approach.

2.2.1. Synchronization

Assume that the position of satellite S, synchronization receiver A, echo receiver B_n and the ground target T are $S(x_s(\eta), y_s(\eta), z_s(\eta))$, $A(x_A, y_A, z_A)$, $B_n(x_{Bn}, y_{Bn}, z_{Bn})$ and $T(x_T, y_T, z_T)$, respectively, where η is the azimuth time.

The signal recorded by receiver A at the azimuth time η_0 and η are expressed as

$$\begin{aligned} S_A(\tau,\eta_0) &= W_r(\tau - R_D(\eta_0)/c)\, W_{aT}(x_s(\eta_0) - x_A)\, W_{aR}(x_s(\eta_0) - x_A) \\ &\quad \times \exp\{-j2\pi f_0 R_D(\eta_0)/c\} \exp\left\{j\pi K_r(\tau - R_D(\eta_0)/c)^2\right\} \quad \tau > R_D(\eta_0)/c - \frac{T_r}{2} + T_1 \quad (1) \\ S_A(\tau,\eta) &= W_r(\tau - R_D(\eta)/c)\, W_{aT}(x_s(\eta) - x_A)\, W_{aR}(x_s(\eta) - x_A) \\ &\quad \times \exp\{-j2\pi f_0 R_D(\eta)/c\} \exp\left\{j\pi K_r(\tau - R_D(\eta)/c)^2\right\} \quad \tau > R_D(\eta)/c - \frac{T_r}{2} + T_2 \quad (2) \end{aligned}$$

where $W_r(\tau)$ is the envelope of transmitted signal pulse, $W_{aT}(\eta)$ the transmitter's antenna beam pattern in azimuth direction, $W_{aR}(\eta)$ the synchronization receiver's antenna beam pattern in azimuth direction, $R_D(\eta)$ the range between the satellite S and the synchronization receiver A at azimuth time η, and T_r the time duration of the chirp signal. T_1 and T_2 are the trigger delays at the azimuth time η_0 and η, respectively.

$$R_D(\eta) = \sqrt{(x_s(\eta) - x_A)^2 + (y_s(\eta) - y_A)^2 + (z_s(\eta) - z_A)^2} \quad (3)$$

In order to obtain more precise expressions, the correlation computation is used in time domain.

$$\begin{aligned} S'(\tau) &= \int_{-\infty}^{+\infty} S_A(t,\eta)\, S_A^*(t-\tau,\eta_0)\, dt \\ &= \int_{-\infty}^{+\infty} \begin{aligned}[t] & W_r'(t - R_D(\eta)/c) \times \exp\{-j2\pi f_0 R_D(\eta)/c\} \times \exp\left\{j\pi K_r(t - R_D(\eta)/c)^2\right\} \\ & \times W_r'(t - \tau - R_D(\eta_0)/c) \times \exp\{j2\pi f_0 R_D(\eta_0)/c\} \times \exp\left\{-j\pi K_r(t - \tau - R_D(\eta_0)/c)^2\right\} \end{aligned} dt \quad (4) \end{aligned}$$

when

$$\tau = \left(R_D\left(\eta\right) - R_D\left(\eta_0\right)\right)/c \tag{5}$$

$S'(\tau)$ reaches the maximum value, which is

$$S'\left(\left[R_D\left(\eta\right) - R_D\left(\eta_0\right)\right]/c\right) = \exp\left\{-j2\pi f_0\left[R_D\left(\eta\right) - R_D\left(\eta_0\right)\right]/c\right\}\int_{-\infty}^{+\infty} W_r'\left(t - R_D\left(\eta\right)/c\right)dt \tag{6}$$

Analysis (6), the angle of $S'([R_D(\eta) - R_D(\eta_0)]/c)$ is $-j2\pi f_0[R_D(\eta) - R_D(\eta_0)]/c$. So $S'_A(\tau,\eta)$ can be obtained by shifting $[R_D(\eta) - R_D(\eta_0)]/c$ of $S_A(\tau,\eta)$ and compensating the phase of $-j2\pi f_0[R_D(\eta) - R_D(\eta_0)]/c$.

$$S'_A\left(\tau,\eta\right) = S_A\left(\tau - \left[R_D\left(\eta\right) - R_D\left(\eta_0\right)\right]/c, \eta_0\right) \times \exp\left\{-j2\pi f_0\left[R_D\left(\eta\right) - R_D\left(\eta_0\right)\right]/c\right\} \tag{7}$$

2.2.2. Range Compression

Then using the reconstruction signal $S'_A(\tau,\eta)$ as a matched filter to compress the echo signal which is received by the echo receiver at azimuth time η, the echo signal of the target $T(x_T, y_T, z_T)$ sampled and recorded by the echo receiver B at azimuth time η is expressed as

$$\begin{aligned} S_B\left(\tau,\eta;x_T,y_T,z_T\right) &= \sigma\left(x_T,y_T,z_T\right) W_r\left(\tau - R_B\left(\eta;x_T,y_T,z_T\right)/c\right) W_{aT}\left(x_s\left(\eta\right) - x_T\right) W_{bi}\left(x_T,y_T,z_T\right) \\ &\quad \times \exp\left\{-j2\pi f_0 R_B\left(\eta;x_T,y_T,z_T\right)/c\right\} \exp\left\{j\pi K_r\left(\tau - R_B\left(\eta;x_T,y_T,z_T\right)/c\right)^2\right\} \end{aligned} \tag{8}$$

$$\begin{aligned} R_B\left(\eta;x_T,y_T,z_T\right) &= R_T\left(\eta;x_T,y_T,z_T\right) + R_R\left(x_T,y_T,z_T\right) \\ &= \sqrt{\left(x_{s1}\left(\eta\right) - x_T\right)^2 + \left(y_{s1}\left(\eta\right) - y_T\right)^2 + \left(z_{s1}\left(\eta\right) - z_T\right)^2} \\ &\quad + \sqrt{\left(x_{B1} - x_T\right)^2 + \left(y_{B1} - y_T\right)^2 + \left(z_{B1} - z_T\right)^2} \end{aligned} \tag{9}$$

where $\sigma(x_T, y_T, z_T)$ is the back scatter coefficient of the target $T(x_T, y_T, z_T)$, $W_r(\tau)$ the envelope of transmitted radar pulse, $W_{aT}(x_s(\eta) - x_T)$ the antenna beam pattern in azimuth direction of the transmitter, $W_{bi}(x_T, y_T, z_T)$ the antenna beam pattern of the ground echo receiver for the target $T(x_T, y_T, z_T)$, $R_T(\eta; x_T, y_T, z_T)$ the range between the satellite S and target $T(x_T, y_T, z_T)$ at Azimuth time η, and $R_R(x_T, y_T, z_T)$ the range between the ground echo receiver A and target $T(x_T, y_T, z_T)$. Here we assume that all the antenna beam patterns are in rectangle functions. The compressed signal is

$$\begin{aligned} S\left(\tau,\eta\right) &= \sigma\left(x_T,y_T,z_T\right) p_r\left(\tau - \left[R_B\left(\eta;x_T,y_T,z_T\right) - R_D\left(\eta\right)\right]/c\right) W_a\left(x_{s1}\left(\eta\right) - x_A\right) \\ &\quad W_{bi}\left(x_T,y_T,z_T\right) W_a\left(x_s\left(\eta\right) - x_T\right) \times \exp\left\{-j2\pi f_0\left[R_B\left(\eta;x_T,y_T,z_T\right) - R_D\left(\eta\right)\right]/c\right\} \\ &= \sigma'\left(\eta;x_T,y_T,z_T\right) \times \exp\left\{-j2\pi f_0 R\left(\eta;x_T,y_T,z_T\right)/c\right\} \end{aligned} \tag{10}$$

where

$$\begin{aligned} R\left(\eta;x_T,y_T,z_T\right) &= R_B\left(\eta;x_T,y_T,z_T\right) - R_D\left(\eta\right) \\ &= \sqrt{\left(x_s\left(\eta\right) - x_T\right)^2 + \left(y_s\left(\eta\right) - y_T\right)^2 + \left(z_s\left(\eta\right) - z_T\right)^2} \\ &\quad - \sqrt{\left(x_s\left(\eta\right) - x_A\right)^2 + \left(y_s\left(\eta\right) - y_A\right)^2 + \left(z_s\left(\eta\right) - z_A\right)^2} \\ &\quad + \sqrt{\left(x_B - x_T\right)^2 + \left(y_B - y_T\right)^2 + \left(z_B - z_T\right)^2} \end{aligned} \tag{11}$$

$$\begin{aligned} \sigma'\left(\eta;x_A,x_T,y_T,z_T\right) &= \sigma\left(x_T,y_T,z_T\right) p_r\left(\tau - R\left(\eta;x_T,y_T,z_T\right)/c\right) \\ &\quad \times W_{aT}\left(x_s\left(\eta\right) - x_A\right) W_{aR}\left(x_s\left(\eta\right) - x_A\right) W_{bi}\left(x_T,y_T,z_T\right) W_{aT}\left(x_s\left(\eta\right) - x_T\right) \end{aligned} \tag{12}$$

2.2.3. Azimuth Compression

Then set the image grid on the ground plane (x_n, y_m) and estimate the average height of the scene z_{ave}. Assume that the intervals of the image grid along the azimuth and range directions are ρ_a and ρ_r.

$$\begin{cases} x_n = n\rho_a & n = 1, 2, \ldots, N \\ y_m = m\rho_r & m = 1, 2, \ldots, M \end{cases} \tag{13}$$

The azimuth focusing formulation is

$$d(n,m) = \sum_{i=0}^{N-1} d_r(i, index(\eta_i; x_n, y_m)) \cdot \phi_c(\eta_i; x_n, y_m) \tag{14}$$

where, $d(n,m)$ is the element of the image, $d_r(i, index(\eta_i; x_n, y_m))$ the element of the range compressed data, $\phi_c(\eta_i; x_n, y_m)$ the compensation phase, and η_i the azimuth time of the i-th range line.

$$index(\eta; x_n, y_m) = \text{round}(R(\eta; x_T, y_T, z_{ave}) F_s \beta / c) \tag{15}$$

$$\phi_c(\eta_i; x_n, y_m) = \exp\{j2\pi f_0 R(\eta; x_T, y_T, z_{ave}) / c\} \tag{16}$$

where, round(X) is a function of rounding the elements of X to the nearest integers, Fs the range sampling rate, and β the range over sample ratio.

3. EXPERIMENT

The experiment uses TerraSAR-X as the transmitter, which works in spotlight mode, and the ground receiver is fixed on the top of a hill near the scene. The system's parameters are listed in Table 1, and the experiment scene is shown in Figure 9. Our ground receiver has one synchronization channel and two echo channels with a vertical baseline, as shown in Figure 9. The two echo channels are used to obtain SAR images and BiInSAR result. The effective vertical baseline of the two echo channels is 2 m. The FM chirp rate and transmitted pulse length are unknown in our experiments.

Table 1. BiSAR experiment parameters.

System parameters	System value
Carrier frequency (GHz)	9.65
Signal bandwidth (MHz)	150
Sample rate (MHz)	725
Pulse repetition frequency	3833

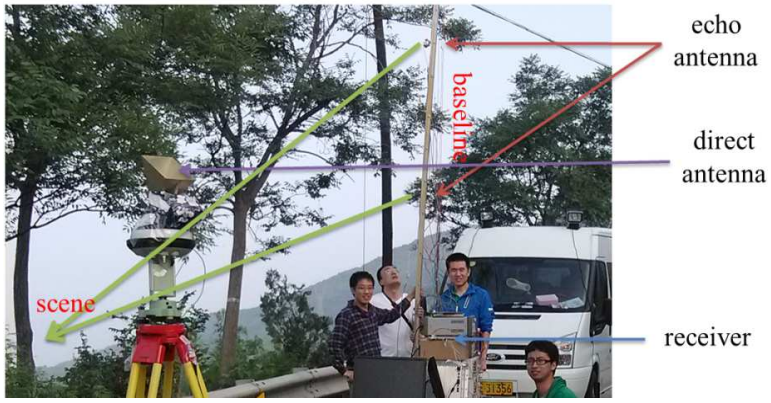

Figure 9. Experiment.

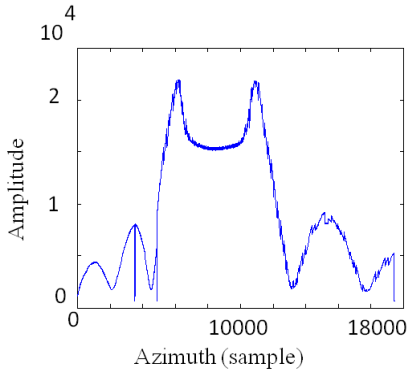

Figure 10. The amplitude of the demodulation complex direct signal.

Figure 10 shows the amplitude of the demodulation complex direct signal. The saturation causes the amplitude reduction in the center of the mainlobe. Because of the variation of the direct signal power, caused by the pattern of the transmitter and receiver antenna, the low GDS, appropriate GDS and high GDS all exist during the exposure time. The sample value and spectrum with low GDS, appropriate GDS and high GDS are shown in Figure 3 to Figure 6. Choose one of the direct signal

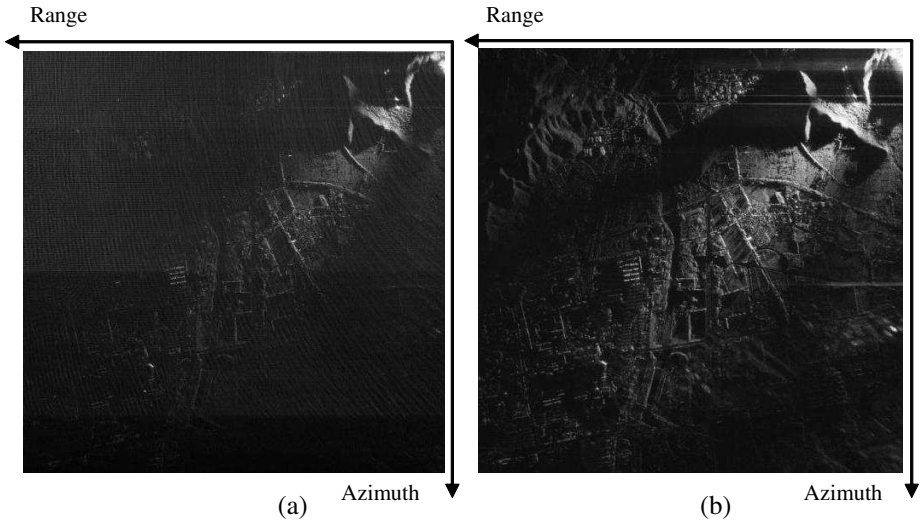

Figure 11. The imaging result. (a) Imaging result using direct signal with saturation as matched filter. (b) Imaging result using reconstructed direct signal as matched filter.

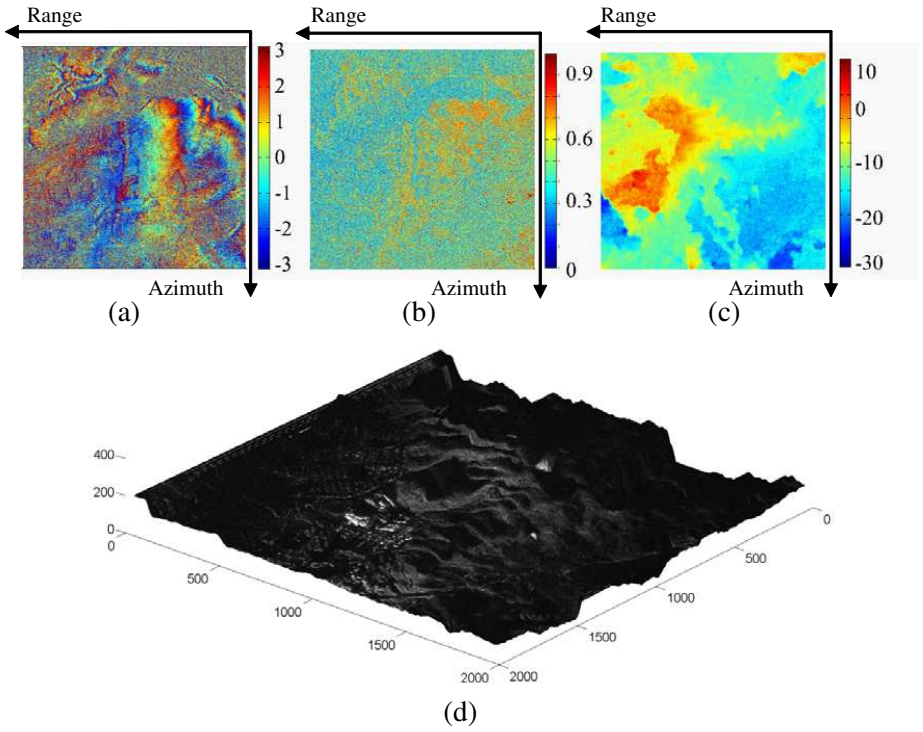

Figure 12. The BiInSAR result. (a) Interferometric phase after interferogram flattening and filtering. (b) Correction coefficient. (c) Unwrapped phase. (d) DEM.

with appropriate gain as the reference signal. Figure 11 is the imaging result. Figure 11(a) shows the imaging result using direct signal with saturation as matched filter. Figure 11(b) shows the imaging result using the match filter which is reconstructed by the proposed method. The results show that the proposed method can resolve the synchronization problem when the direct signal is unsatisfactory, and the parameters of the chirp are unknown.

Figure 12 shows the BiInSAR result. The processes of the BiInSAR include imaging, coregistration,

interferogram generation, interferogram flattening, filtering, phase unwrapping and phase to height conversion [7–10]. Figure 12(a) is the interferometric phase after interferogram flattening and filtering. The filtering step uses pyramid nonlocal means filter algorithm [21]. Figure 12(b) is the correction coefficient, and Figure 12(c) is the unwrapped phase result of the hill area of the scene. The unwrapping step uses region growing algorithm [21]. Figure 12(d) is the digital elevation model (DEM). The results show that the BiSAR imaging results obtained by the proposed synchronization method can be used in BiInSAR.

4. CONCLUSION

This paper proposes a modified synchronization approach to make the synchronization practicable in the situation when the direct signal is unsatisfactory, and the parameters of the transmitted signal are even unknown. Both the experiment results of imaging and BiInSAR results verified the effectiveness of the proposed approach.

ACKNOWLEDGMENT

This work is funded jointly by the DLR (German Aerospace Centre) Project (grant number MTH1517) and the "Hundred Talents Program" of the Chinese Academy of Sciences, which is seen as a key item of their work and gratefully acknowledged.

REFERENCES

1. Wu, B.-I., M. C. Yeung, Y. Hara, and J. A. Kong, "InSAR height inversion by using 3-D phase projection with multiple baselines," *Progress In Electromagnetics Research*, Vol. 91, 173–193, 2009.
2. Liu, D., Y. Du, G. Sun, W.-Z. Yan, and B.-I. Wu, "Analysis of InSAR sensitivity to forest structure based on radar scattering model," *Progress In Electromagnetics Research*, Vol. 84, 149–171, 2008.
3. Sabry, R. and P. W. Vachon, "Advanced polarimetric synthetic aperture radar (SAR) and electro-optical (EO) data fusion through unified coherent formulation of the scattered EM field," *Progress In Electromagnetics Research*, Vol. 84, 189–203, 2008.
4. Tan, C.-P., J.-Y. Koay, K.-S. Lim, H.-T. Ewe, and H.-T. Chuah, "Classification of multi-temporal SAR images for rice crops using combined entropy decomposition and support vector machine technique," *Progress In Electromagnetics Research*, Vol. 71, 19–39, 2007.
5. Ballester-Berman, J. D., F. Vicente-Guijalba, and J. M. Lopez-Sanchez, "Polarimetric SAR model for soil moisture estimation over vineyards at C-band," *Progress In Electromagnetics Research*, Vol. 142, 639–665, 2013.
6. Zhang, X., J. Qin, and G. Li, "SAR target classification using bayesian compressive sensing with scattering centers features," *Progress In Electromagnetics Research*, Vol. 136, 385–407, 2013.
7. Reuter, S., F. Behner, H. Nies, O. Loffeld, D. Matth, and J. Schiller, "Development and experiments of a passive SAR receiver system in a bistatic spaceborne/stationary configuration," *Proc. IEEE IGARSS*, 118–121, 2010.
8. Ben Kassem, M. J., J. Saillard, and A. Khenchaf, "BISAR mapping I: Theory and modelling," *Progress In Electromagnetics Research*, Vol. 61, 39–65, 2006.
9. Ben Kassem, M. J., J. Saillard, and A. Khenchaf, "BISAR mapping II: Treatment, simulation and experimentation," *Progress In Electromagnetics Research*, Vol. 61, 67–87, 2006.
10. Duque, S., P. Lopez-Dekker, and J. J. Mallorqui, "Single-pass bistatic SAR interferometry using fixed-receiver configurations: Theory and experimental validation," *IEEE Trans. Geosci. Remote Sens.*, Vol. 48, No. 6, 2740–2749, Jun. 2010.
11. Rui, L., J. Xiong, and Y. Huang, "Analysis of bistatic SAR frequency synchronization," *ICCCAS*, Vol. 1, 380–383, Jun. 2006.
12. Sun, C., L. Zhou, D. Zhang, G. Lu, and W. Chen, "Analysis of phase synchronization errors based on distributed small satellite SAR system," *ISAPE*, 1–4, Oct. 2006.

13. Dekker, P. L., J. J. Mallorquí, P. S. Morales, and J. S. Marcos, "Phase synchronization and doppler centroid estimation in fixed receiver bistatic SAR systems," *IEEE Trans. Geosci. Remote Sens.*, Vol. 46, No. 11, 3459–2471, Nov. 2008.
14. Zhang, Y., D. Liang, and Z. Dong, "Analysis of time and frequency synchronization errors in spaceborne parasitic InSAR system," *Proc. IEEE IGARSS*, 3047–3050, 2006.
15. Breit, H., M. Younis, U. Balss, A. Niedermeier, C. Grigorov, J. Hueso-Gonzalez, G. Krieger, M. Eineder, and T. Fritz, "Bistatic synchronization and processing of Tandem-X data," *Proc. IEEE IGARSS*, 2424–2427, 2011.
16. Lopez-Dekker, P., J. Mallorqui, P. Serra-Morales, and J. Sanz-Marcos, "Phase synchronization and doppler centroid estimation in fixed receiver bistatic SAR systems," *IEEE Trans. Geosci. Remote Sens.*, Vol. 46, No. 11, 3459–3471, Nov. 2008.
17. López-Dekker, P., J. J. Mallorqui, P. Serra-Morales, and J. Sanz-Marcos, "Phase and temporal synchronization in bistatic SAR systems using sources of opportunity," *Proc. IEEE IGARSS*, 97–100, Jul. 2007.
18. Rodriguez-Cassola, M., S. V. Baumgartner, G. Krieger, and A. Moreira, "Bistatic TerraSAR-X/F-SAR spaceborne-airborne SAR experiment: Description, data processing, and results," *IEEE Trans. Geosci. Remote Sens.*, Vol. 48, No. 2, 781–790, Feb. 2010.
19. Walterscheid, I., T. Espeter, A. R. Brenner, J. Klare, J. H. G. Ender, H. Nies, R. Wang, and O. Loffeld, "Bistatic SAR experiments with PAMIR and TerraSAR-X — Setup, processing, and image results," *IEEE Trans. Geosci. Remote Sens.*, Vol. 48, No. 8, 3268–3279, Aug. 2010.
20. Wang, R., Y. Deng, Z. Zhang, and Y. Shao, "Double-channel bistatic SAR system with spaceborne illuminator for 2-D and 3-D SAR remote sensing," *IEEE Trans. Geosci. Remote Sens.*, 4496–4507, Aug. 2013.
21. Chen, R., W. Yu, R. Wang, G. Liu, and Y. Shao, "Interferometric phase denoising by pyramid nonlocal means filter," *IEEE. Geosci. Remote Sens. Lett.*, Vol. 10, No. 4, 826–830, Jul. 2013.